

A realistic non-local heat engine based on Coulomb coupled systems

Aniket Singha

Department of Electronics and Electrical Communication Engineering,
Indian Institute of Technology Kharagpur,
Kharagpur-721302, India

Optimal non-local heat-engines, based on Coulomb-coupled systems, demand a sharp step-like change in energy resolved system-to-reservoir coupling around the ground state of quantum-dots [1–5]. Such sharp step-like transition in the system-to-reservoir coupling cannot be achieved in a realistic scenario. Here, I propose realistic design for non-local heat engine based on Coulomb-coupled systems. The performance of the proposed heat engine is then theoretically investigated using quantum-master-equation (QME) approach. It is demonstrated that the theoretical maximum power output for the proposed set-up is limited to about 50% of the optimal design. Despite a lower performance compared to the optimal set-up, the novelty of the proposed design is the conjunction of fabrication simplicity along with reasonable power output. At the end, the sequential transport processes leading to a performance deterioration of the proposed design strategy are analyzed and a method to alleviate such transport processes is proposed. The design proposed in this paper can be used to fabricate high-performance non-local cryogenic heat engines.

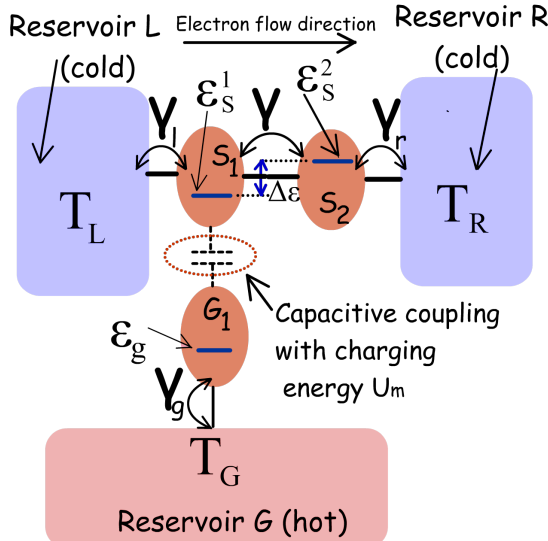


FIG. 1. Schematic diagram of the proposed non-local heat engine based on Coulomb-coupled quantum dots. The entire system consists of three dots S_1 , S_2 and G_1 which are electrically coupled to the reservoirs L , R and G respectively. The dots S_1 and S_2 are tunnel coupled, while S_1 and G_1 are electrostatically coupled. The ground states of S_1 and S_2 form a staircase configuration with $\varepsilon_s^2 \approx \varepsilon_s^1 + \Delta\varepsilon$. In the proposed arrangement, current can be driven between the cold reservoirs L and R by absorbing thermal energy from the hot reservoir G .

I. INTRODUCTION

With the progress in fabrication and scaling technology, efficient heat harvesting in lower dimensional systems has gained a lot of attention [6–16]. One of the major issues affecting heat harvesting performance in nano-systems is the drastic lattice heat flux resulting from a small spatial separation between the heat

reservoir and the heat sink. The large lattice heat flux severely limits the overall efficiency of the heat engine and poses a major performance issue in cases where supply of heat energy is limited. Tailoring the lattice thermal conductance, in an attempt to gain enhanced harvesting efficiency generally affects the current path, thereby deteriorating the peak harvested power. As such, one of the crucial focus of the modern thermoelectric community is to facilitate an independent optimization of the electron transport path and lattice heat conduction path, by introducing a spatial separation between the current path and the heat reservoir [17–19]. This phenomenon of harvesting heat from a reservoir, which is spatially separated from the current conduction path, is known as non-local heat harvesting [1–5, 17–20]. In this case, tailoring the lattice heat transport path, in an attempt to gain enhanced efficiency, can be accomplished without altering the current conduction path. Recently designs and concepts of non-local heat engines and refrigerators using Coulomb coupled quantum dots have been proposed and explored in literature [1–5, 20]. However, the operation of such non-local heat engines demand a sharp step-like change in the system-to-reservoir coupling around the ground state energy [1–5, 20], which is impossible to achieve in a practical scenario. In this paper, I propose a realistic design strategy to accomplish non-local heat harvesting using capacitively coupled quantum dots. Unlike the optimal non-local heat-engine based on Coulomb coupled systems [1–5, 20], the proposed design doesn't demand an change in the system-to-reservoir coupling near the ground state. The performance proposed heat-engine is then evaluated and compared with the optimal set-up. It is demonstrated that the performance of the proposed heat engine hovers around 50% of the optimal set-up. However, the novelty of the proposed set-up is the conjunction of fabrication simplicity along with a reasonable power output. At the end, the

processes leading to a performance deterioration of the proposed set-up is discussed and analyzed. This paper is organized as follows. In Sec. II, I illustrate the proposed design strategy and elaborate the transport formulation employed to analyze the thermoelectric performance of the same. Next, Sec III elaborates a detailed analysis on the heat harvesting performance and regime of operation of the proposed heat-engine. A performance comparison between the proposed heat engine and the optimal set-up is also conducted along with a brief discussion on the transport processes leading to a performance deterioration of the proposed heat engine. I conclude this paper briefly in Sec. IV

II. PROPOSED DESIGN AND TRANSPORT FORMULATION

The proposed heat engine, schematically demonstrated in Fig. 1, consists of three dots S_1 , S_2 and G_1 which are electrically coupled to the reservoirs L , R and G respectively. S_1 and S_2 are tunnel coupled to each other, while G_1 is capacitively coupled to S_1 . The ground states of S_1 and S_2 form a stair-case configuration with $\varepsilon_s^2 \approx \varepsilon_s^1 + \Delta\varepsilon$. Any electronic tunneling between the dots S_1 and G_1 is suppressed via suitable fabrication techniques. Energy exchange between the two dots is, however, possible via capacitive coupling [21–23]. Quantum dots that are far from each other in space, may be bridged to obtain strong capacitive coupling, in addition to excellent thermal isolation between the hot and cold reservoirs [21, 22]. In addition, the bridge may be fabricated between two specific quantum dots to drastically enhance their mutual capacitive coupling, without affecting the electrostatic energy of the other quantum dots [21–23]. Thus, the change in electron number n_{S_1} (n_{G_1}) of the dot S_1 (G_1) influences the electrostatic energy of the dot G_1 (S_1). In general, the total electrostatic energy U of the system, demonstrated in Fig. 1 (a), consisting of three dots can be given by:

$$U(n_{S_1}, n_{G_1}, n_{S_2}) = \sum_x U_x^{self} \left(n_x - \frac{V_x C_x^{self}}{q} \right)^2 + \sum_{(x_1, x_2)}^{x_1 \neq x_2} U_{x_1, x_2}^m \left(n_{x_1} - \frac{V_{x_1} C_{x_1}^{self}}{q} \right) \left(n_{x_2} - \frac{V_{x_2} C_{x_2}^{self}}{q} \right),$$

where n_x is the electron number, C_x^{self} is the self-capacitance and $U_x^{self} = \frac{q^2}{C_x^{self}}$ is the electrostatic energy due to self-capacitance of quantum dot ‘ x ’. U_{x_1, x_2}^m is the electrostatic energy arising out of Coulomb coupling between two different quantum dots that are separated in space. Here, a minimal physics based model is used to investigate the heat engine performance under the assumption that the change in potential due self-capacitance is much greater than than the average thermal voltage kT/q or the applied bias voltage V , that is $U_x^{self} = \frac{q^2}{C_x^{self}} \gg (kT, qV)$. Hence, electron occupation probability or transfer rate via the Coulomb blocked energy level, due to self-capacitance, is negligibly small. The analysis of the entire system of dots may hence be approximated by limiting the maximum number of electrons in each dot to one. Thus the analysis of the entire system may be limited to eight multi-electron levels, which I denote by the electron occupation number in the ground state of each quantum dot. Hence, a possible state of interest in the system may be denoted as $|n_{S_1}, n_{G_1}, n_{S_2}\rangle = |n_{S_1}\rangle \otimes |n_{G_1}\rangle \otimes |n_{S_2}\rangle$, where $n_{S_1}, n_{G_1}, n_{S_2} \in (0, 1)$. I also assume that the electrostatic coupling between S_1 , S_2 and between S_2 , G_1 is negligible, such that, for all practical purposes under consideration, $U_{S_1, S_2}^m \approx 0$ and $U_{G_1, S_2}^m \approx 0$. Since, the electronic transport and ground states in S_1 and G_1 are mutually coupled, I treat the pair of dots S_1 and G_1 as a sub-system (ς_1), S_2 being the complementary sub-system (ς_2) of the entire system consisting of three dots [24]. The state probability of ς_1 is denoted by $P_{i,j}^{\varsigma_1}$, i and j being the number of electrons in the dot S_1 and G_1 respectively. $P_k^{\varsigma_2}$, on the other hand, denotes the probability of occupancy of the dot S_2 in the sub-system ς_2 . It can be shown that if $\Delta\varepsilon$ is much greater than the ground state broadening due to system-to-reservoir coupling, then the interdot tunneling rate between S_1 and S_2 is optimized when $\varepsilon_s^1 + U_{S_1, G_1}^m = \varepsilon_s^2$, that is when $\Delta\varepsilon = U_{S_1, G_1}^m$ [24]. To evaluate the optimal performance of the proposed heat-engine, I hence assume $\Delta\varepsilon = U_{S_1, G_1}^m$ [24]. Henceforth, I would simply represent U_{S_1, G_1}^m as U_m . Under the assumption stated above, the equations governing sub-system state probabilities in steady state can be derived as [24]:

$$\begin{aligned} -P_{0,0}^{\varsigma_1} \{f_L(\varepsilon_s^1) + f_G(\varepsilon_g^1)\} + P_{0,1}^{\varsigma_1} \{1 - f_G(\varepsilon_g^1)\} + P_{1,0}^{\varsigma_1} \{1 - f_L(\varepsilon_s^1)\} &= 0 \\ -P_{1,0}^{\varsigma_1} \{1 - f_L(\varepsilon_s^1) + f_G(\varepsilon_g^1 + U_m)\} + P_{1,1}^{\varsigma_1} \{1 - f_G(\varepsilon_g^1 + U_m)\} + P_{0,0}^{\varsigma_1} f_G(\varepsilon_g^1) \\ -P_{0,1}^{\varsigma_1} \left\{ 1 - f_g(\varepsilon_g^1) + f_L(\varepsilon_s^1 + U_m) + \frac{\gamma}{\gamma_c} P_1^{\varsigma_2} \right\} + P_{0,0}^{\varsigma_1} f_G(\varepsilon_g^1) + P_{1,1}^{\varsigma_1} \left\{ 1 - f_L(\varepsilon_s^1 + U_m) + \frac{\gamma}{\gamma_c} P_0^{\varsigma_2} \right\} &= 0 \\ -P_{1,1}^{\varsigma_1} \left\{ [1 - f_g(\varepsilon_g^1 + U_m)] + [1 - f_L(\varepsilon_s^1 + U_m)] + \frac{\gamma}{\gamma_c} P_0^{\varsigma_2} \right\} + P_{1,0}^{\varsigma_1} f_G(\varepsilon_g^1 + U_m) + P_{0,1}^{\varsigma_1} \left\{ f_L(\varepsilon_s^1 + U_m) + \frac{\gamma}{\gamma_c} P_1^{\varsigma_2} \right\} &= 0 \quad (1) \end{aligned}$$

$$\begin{aligned} -P_0^{\varsigma_2} \{f_R(\varepsilon_s^2) + \frac{\gamma}{\gamma_c} P_{1,1}^{\varsigma_1}\} + P_1^{\varsigma_2} \left\{ 1 - f_R(\varepsilon_s^2) + \frac{\gamma}{\gamma_c} P_{0,1}^{\varsigma_1} \right\} &= 0 \\ -P_1^{\varsigma_2} \{1 - f_R(\varepsilon_s^2) + \frac{\gamma}{\gamma_c} P_{0,1}^{\varsigma_1}\} + P_0^{\varsigma_2} \left\{ f_R(\varepsilon_s^2) + \frac{\gamma}{\gamma_c} P_{1,1}^{\varsigma_1} \right\} &= 0, \quad (2) \end{aligned}$$

where γ_c and γ are related to the reservoir-to-system

tunnel coupling and the inter-dot tunnel coupling respectively [24, 25]. In the above set of equations, $f_\lambda(\varepsilon)$ denote the probability of occupancy of the reservoir λ at energy ε . For the purpose of calculations in this paper, I assume an equilibrium Fermi-Dirac statistics at the reservoirs. From the set of Eqns. (1) and (2), it is clear that an electron in S_1 can tunnel into S_2 only when the ground state in the dot G_1 is occupied with an electron. The set of Eqns. (1) and (2) are coupled to each other and may be solved using any iterative method. Here, I use Newton-Raphson iterative method to solve the steady-state values of sub-system probabilities. On calculation of the sub-system state probabilities $P_{i,j}^{S_1}$ and $P_k^{S_2}$, the electron current flow into (out of) the system from the reservoirs $L(R)$ can be given as:

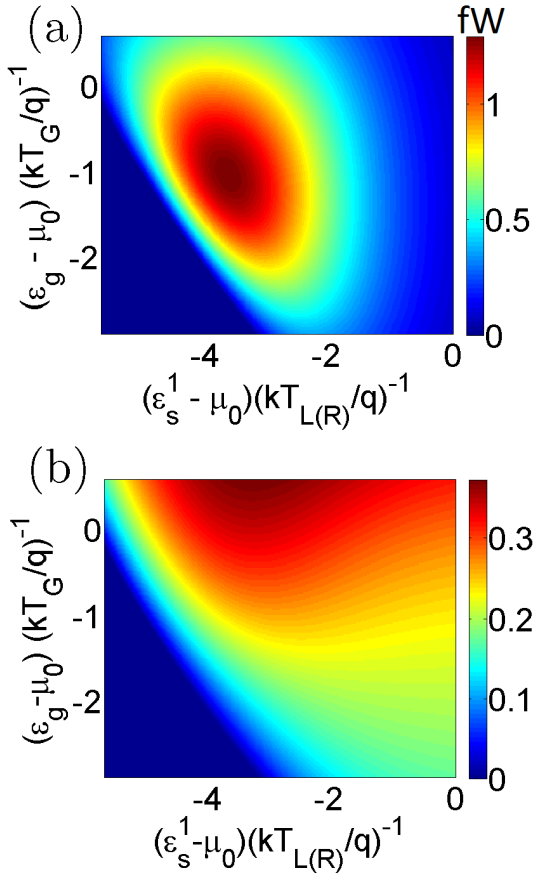


FIG. 2. Variation of the proposed heat engine performance with variation in the the ground states ε_g and ε_s^1 for $U_m = 3.9\text{meV}$ ($\approx 6\frac{kT}{q}$) and $V = 1.3\text{meV}$ ($\approx 2\frac{kT}{q}$). Colour plot demonstrating the variation in (a) generated power (P) and (b) efficiency η/η_c . $T = \frac{T_{L(R)}+T_G}{2} = 7.5K$ is the average temperature between the heat source and the heat sink. The efficiency of generation is measured with respect to the Carnot efficiency $\eta_c = 1 - T_{L(R)}/T_G$

$$I_L = q\gamma_c \times \{P_{0,0}^{S_1}f_L(\varepsilon_s^1) + P_{0,1}^{S_1}f_L(\varepsilon_s^1 + U_m)\} - q\gamma_c P_{1,0}^{S_1}\{1 - f_L(\varepsilon_s^1)\} - q\gamma_c P_{1,1}^{S_1}\{1 - f_L(\varepsilon_s^1 + U_m)\}$$

$$I_R = -q\gamma_c \times \{P_0^{S_2}f_R(\varepsilon_s^1) - P_1^{S_2}\{1 - f_R(\varepsilon_s^1)\}\}, \quad (3)$$

Next, I use the set of Eqns. (1), (2) and (3), to evaluate the thermoelectric generation performance of the the set-up demonstrated in Fig. 1. To analyze the performance of the heat engine, I use a voltage-controlled set-up demonstrated in literature [26–28], where an applied bias voltage V is used to emulate the voltage drop across an external load. Assuming the equilibrium electrochemical potential across the entire set-up is μ_0 , and a voltage drop V across the external load, the quasi-Fermi levels at the reservoirs L and R may be written as $\mu_{L(R)} = \mu_0 \pm \frac{V}{2}$. The generated power (P) and efficiency (η) can be defined as:

$$P = I_{L(R)} \times V,$$

$$\eta = \frac{P}{I_Q}, \quad (4)$$

where V is the applied potential bias in the voltage controlled model and I_Q is the sum of electronic and lattice heat flux from the heat source (G). In the non-local heat engine the lattice heat flux can be favourably engineered [29–33] without affecting the current conduction path. In addition the lattice heat flux is generally independent of the system configuration [34–41]. Hence, to simplify our calculation, we assume ideal condition by neglecting the lattice heat flux as done in recent literature [6, 7, 42, 43]. The generation efficiency for our case, can hence be defined as:

$$\eta = \frac{P}{I_{Q_e}}, \quad (5)$$

where the electronic heat flux at the heat source I_{Q_e} can be calculated as [24]:

$$I_{Q_e} = U_m \gamma_c \{P_{10}^{S_1} f_G(\varepsilon_g + U_m) - P_{11}^{S_1} \{1 - f_G(\varepsilon_g + U_m)\}\} \quad (6)$$

Interestingly Eqn. (6) is not directly dependent on ε_g . This is due to the fact that the net electronic current into or out of the reservoir G is zero. To better understand this, let us consider the situation where an electron tunnels into G_1 from G with an energy $\varepsilon_g + U_m$, when the ground state of S_1 is occupied. Next, the electron tunnels out of S_1 with an energy $\varepsilon_s^1 + U_m$, followed by the electron tunneling out of G_1 with an energy ε_g . In this process a heat packet U_m is lost from G , independent of μ_0 . Without loss of generality, I assume that $\gamma_c = 10^{-6}\frac{q}{h}$ and $\gamma = 10^{-5}\frac{q}{h}$. The temperature of the reservoirs $L(R)$ and G are assumed to be $T_{L(R)} = 5K$ and $T_G = 10K$. The average temperature bewteen the hot and the cold reservoirs is, hence, given by $T = \frac{T_{L(R)}+T_G}{2} = 7.5K$.

III. RESULTS

In this section, I discuss the optimal operation regimes of the proposed heat engine. In addition, I conduct a performance comparison of the proposed heat engine

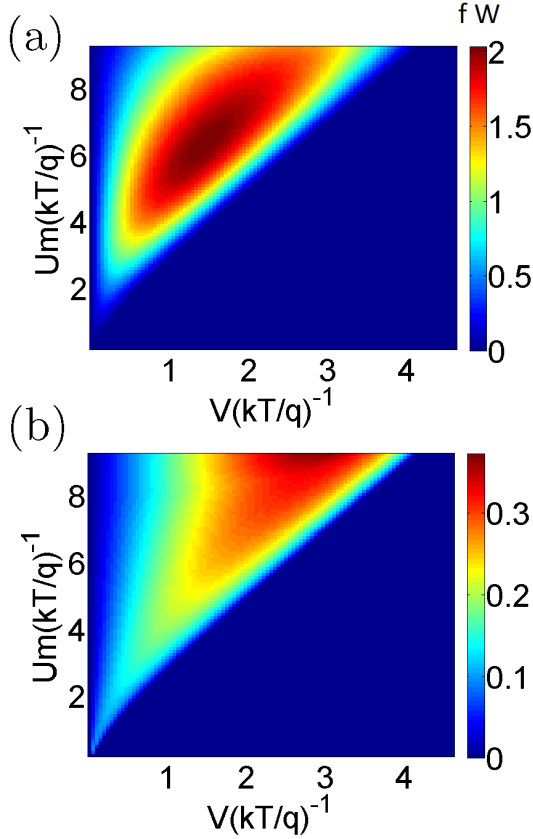


FIG. 3. Variation in the peak performance of the heat engine with variation in Coulomb coupling energy U_m and applied bias V . Colour plot depicting the (a) peak generated power P_M and (b) efficiency at the peak generated power for a range of values of V and U_m . To find out the maximum power P_M for a given value of V and U_m , the ground states of the dots are tuned to optimal position. $T = \frac{T_{L(R)} + T_G}{2} = 7.5K$ is the average temperature between the heat source and the heat sink. The efficiency of maximum power (P_M) generation is normalized with respect to the Carnot efficiency $\eta_c = 1 - T_{L(R)}/T_G$

with the optimal set-up discussed in literature and investigate the transport processes leading to a performance deterioration of the proposed set-up. Fig. 2 demonstrates the performance of the heat engine, in particular the generated power P and efficiency of generated power (η/η_c) over a range of the positions of the ground states ε_g and ε_s^1 for $U_m = 3.9meV$ ($\approx 6\frac{kT}{q}$) and $V = 1.3meV$ ($\approx 2\frac{kT}{q}$). It can be noted that the regime of heat harvesting corresponds to $\varepsilon_s^1 + U_m - \mu_0$ lying within a few kT , that is $-few\ kT_{L(R)} < \varepsilon_s^1 + U_m - \mu_0 < few\ kT_{L(R)}$. Such a behaviour can be expected since net interdot electron flow is optimized when $\varepsilon_s^2 = \varepsilon_s^1 + U_m$ lies within a window of a few $kT_{L(R)}$ around the equilibrium Fermi-energy. Similarly, it can also be noted that for heat harvesting, the ground state ε_g must lie within a few kT_G of the equilibrium Fermi energy μ_0 . This can be understood by the following: if $\varepsilon_g - \mu_0 < -few\ kT_G$, then the ground

state ε_g is always occupied with an electron and so the asymmetry of the system with respect to the reservoir L and R disappears. Hence a directional thermoelectric current flow is not possible [5]. On the other hand, when $\varepsilon_g - \mu_0 > few\ kT_G$, the probability of an electron tunneling into the reservoir G_1 with an energy $\varepsilon_g + U_m$ (provided that the ground state of S_1 is occupied) is negligibly small, resulting in the deterioration of the unidirectional current flow and hence, power generation. Fig. 2(b) demonstrates the heat engine efficiency as a function of the ground state energy levels. The efficiency of heat harvesting increases monotonically with increase in $\varepsilon_g - \mu_0$. An equivalent behaviour can be noted in bulk and lower dimensional thermoelectric engines as the equilibrium Fermi-energy moves outside the band-edge [6, 7, 12, 42, 43]. The variation in generation efficiency with ε_s^1 is non-monotonic. Initially as ε_s^1 increases and approaches the Fermi energy, the generated power increases leading to an increase in efficiency. As ε_s^1 gradually increases the probability of reverse electronic flow from the system to reservoir L at energy $\varepsilon_s^1 + U_m$ increases. Such processes (discussed later) lead to a deterioration in the generation efficiency. The variation of the optimal performance of the heat engine with variation in the Coulomb coupling energy U_m and applied bias V is demonstrated in Fig. 3. In particular, Fig. 3 (a) demonstrates the maximum generated power (P_M), while Fig. 3 (b) demonstrates the efficiency at the maximum generated power for a range of values of the applied bias V and the Coulomb coupling energy U_m . To calculate the the maximum generated power P_M for a given value of V and U_m , the ground states of the dots are tuned to the optimal energy position. It should be noted that the maximum generated power is low for low values of U_m . This is due to the fact that the ground state of the dots approach symmetrical arrangement with respect to the reservoir L and R as U_m approaches towards zero. Hence, the directional flow of electrons decreases. As U_m increases, the asymmetry of the system increases resulting in an increase in directional electron flow, and hence, the maximum generated power [5]. With further increase in U_m , the maximum generated power reaches its peak and then decreases due to lower probability of an electron tunneling into G_1 with an energy $\varepsilon_g + U_m$, when the ground state of S_1 is already occupied. For a fixed value of U_m , the maximum generated power first increases and then decreases with an increase in the bias voltage V . Such a behaviour is indeed expected from heat engines as the regime of operation approaches from short-circuited condition to the open-circuited condition [28]. Fig. 3(b) demonstrates the efficiency at the maximum generated power with variation in applied bias V and Coulomb coupling energy U_m . The efficiency varies non-monotonically with the applied bias V , that is, the efficiency increases with an increase in V as the regime of operation approaches the point of maximum power and then gradually decreases as the generated power

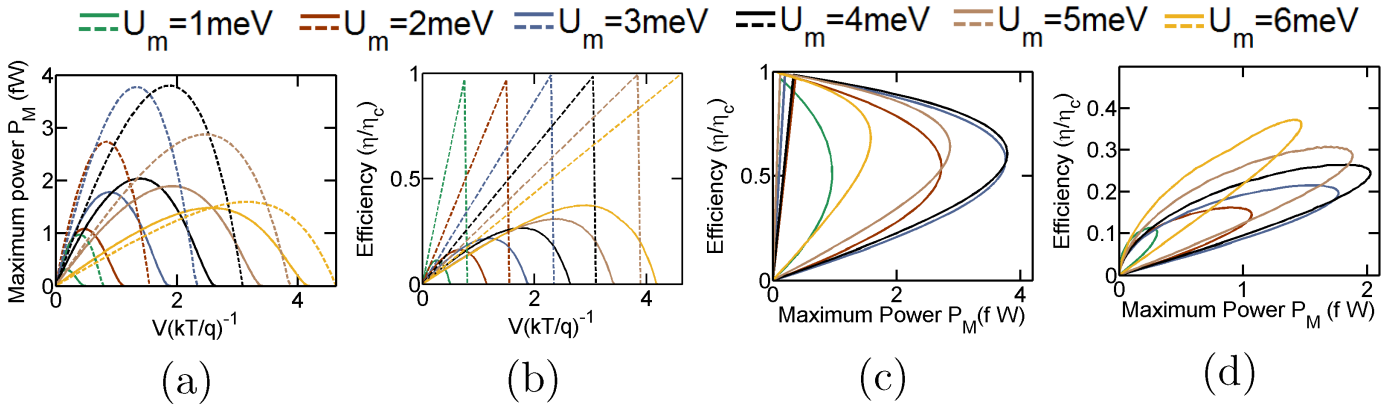


FIG. 4. Performance comparison of the proposed non-local heat engine (solid lines) with the optimal set-up [1–4] (dashed lines) for different values of the Coulomb coupling energy. Plot of (a) maximum generated power P_M vs bias voltage V , (b) efficiency (with respect to Carnot efficiency) at the maximum generated power vs bias voltage, (c) maximum power P_M vs efficiency at the maximum power for the optimal set-up (d) maximum power P_M vs efficiency at the maximum power for the proposed design.

decreases with the regime of operation approaching the open circuited condition. Such a trend can also be noted in bulk and lower dimensional heat engines [6, 7]. On the other hand with an increase in U_m , the efficiency at the maximum power increases monotonically as $\varepsilon_g + U_m$ gradually surpasses the Fermi energy. An equivalent trend, again, can be noted in bulk and lower dimensional thermoelectric engines as the band-edge gradually surpasses the Fermi-energy [6, 26–28, 44]. Fig. 4 demonstrates a performance comparison of the proposed heat engine with the optimal non-local heat engine put forward in literature [1–4]. In particular, Fig. 4(a) and (b) demonstrates the variation in the maximum power P_M and efficiency at the maximum power respectively with applied load bias V for different values of U_m . We note that the overall maximum generated power for the proposed design P_{MAX}^{prop} is approximately $2.03fW$, which is about 50% of the overall maximum power output of $3.8fW$ for the optimal design P_{MAX}^{opt} . In both these cases the maximum power is generated around $U_m \approx 4meV$. As already discussed in literature [5], the efficiency at the overall maximum generated power for the optimal set-up increases linearly with the applied bias for a given value of U_m . The efficiency at the overall maximum power for our proposed design and the optimal set-up are 24.5% and 60% of the Carnot efficiency respectively. In addition, it can also be noted that the open circuit voltage for the optimal set-up is slightly higher compared to the proposed design. Fig. 4 (c) and (d) demonstrates the the maximum power vs efficiency loops [6] for the optimal design and the proposed design respectively for various values of U_m . We note that the power-efficiency trade-off for the optimal set-up is somewhat mild compared to the proposed design.

I end the discussion with a brief description of the processes leading to a deterioration in generated power and

efficiency for the proposed set-up. First, let us consider the cycles leading to electron transport from the reservoir L to the reservoir R against the applied bias while absorbing a heat packet U_m from reservoir G . Let us consider the cycle $(n_{S_1}, n_{G_1}, n_{S_2}) \rightarrow (n_{S_1} + 1, n_{G_1}, n_{S_2}) \rightarrow (n_{S_1} + 1, n_{G_1} + 1, n_{S_2}) \rightarrow (n_{S_1}, n_{G_1} + 1, n_{S_2} + 1) \rightarrow (n_{S_1}, n_{G_1}, n_{S_2} + 1) \rightarrow (n_{S_1}, n_{G_1}, n_{S_2})$. In this cycle, the system starts with an initial state with the unoccupied ground state in all the three quantum dots. An electron tunnels from L into S_1 at energy ε_s^1 , followed by an electron tunneling into G_1 from G at energy $\varepsilon_g + U_m$. At the next instant, the electron in S_1 tunnels into S_2 , after which the electron in G_1 tunnels out into G with energy ε_g . The cycle is completed and the system returns to the initial state when the electron in S_2 tunnels out into the reservoir R with an energy $\varepsilon_s^2 = \varepsilon_s^1 + U_m$. It is clear that in this process an electron is transferred from L to R while absorbing a heat packet U_m from G . Another cycle that again transfers electrons from L to R , while absorbing heat packet from G can be given by $(n_{S_1}, n_{G_1}, n_{S_2}) \rightarrow (n_{S_1} + 1, n_{G_1}, n_{S_2}) \rightarrow (n_{S_1} + 1, n_{G_1} + 1, n_{S_2}) \rightarrow (n_{S_1}, n_{G_1} + 1, n_{S_2} + 1) \rightarrow (n_{S_1}, n_{G_1} + 1, n_{S_2}) \rightarrow (n_{S_1}, n_{G_1}, n_{S_2})$. These transport processes contribute to thermoelectric power generation while absorbing heat energy from G . Next, consider the cycle $(n_{S_1}, n_{G_1}, n_{S_2}) \rightarrow (n_{S_1} + 1, n_{G_1}, n_{S_2}) \rightarrow (n_{S_1} + 1, n_{G_1} + 1, n_{S_2}) \rightarrow (n_{S_1}, n_{G_1} + 1, n_{S_2}) \rightarrow (n_{S_1}, n_{G_1}, n_{S_2})$. This cycle consists of an electron tunneling into S_1 from L , with an energy ε_s^1 , followed by an electron tunneling into G_1 with an energy $\varepsilon_g + U_m$. At the next step, the electron in S_1 exits into reservoir L with an energy $\varepsilon_s^1 + U_m$. The cycle is completed with the electron in G_1 tunnels out into G with energy ε_g . It is evident that in this process, a packet of heat energy U_m is transmitted from reservoir G to L without any net flow of electrons between L and R . So, effectively the heat packet U_m is wasted without any power conversion.

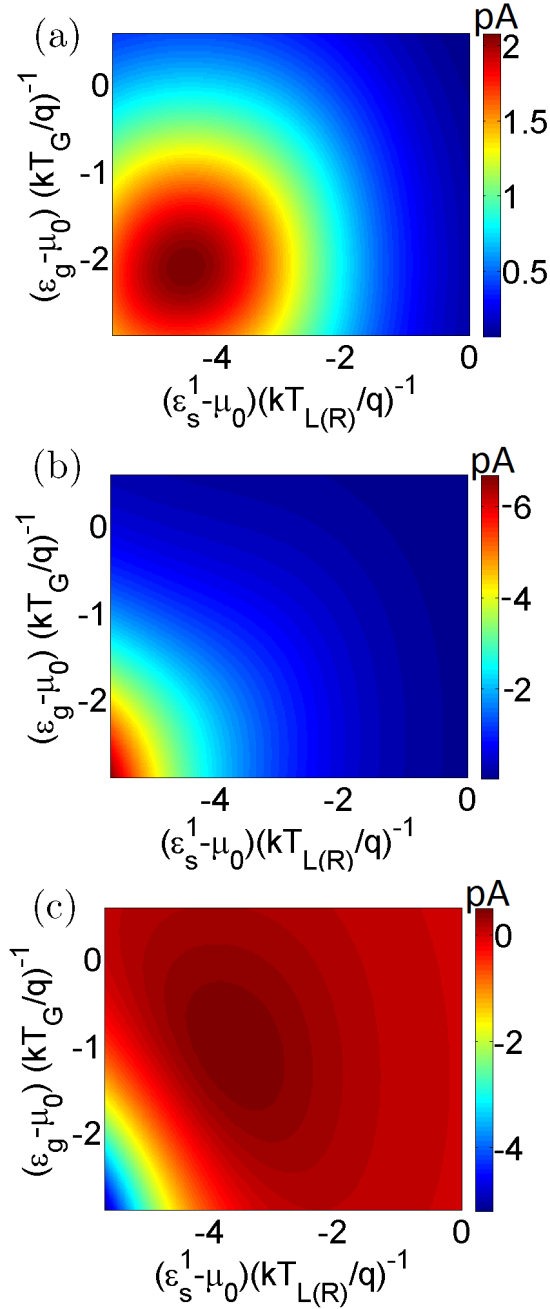


FIG. 5. Colour plots demonstrating the electron flow into the system from the reservoir L with variation in the the ground states ε_g and ε_s^1 , for $U_m = 3.9\text{meV} (\approx 6\frac{kT}{q})$ and $V = 1.3\text{meV} (\approx 2\frac{kT}{q})$, when the (a) ground state of the dot G_1 is not occupied (b) ground state of the dot is occupied (c) total average current between the system and the reservoir L . Interestingly, when the ground state of the dot G_1 is occupied, the net electronic flow is directed from the system into the reservoir L . Since, the net direction of current for thermoelectric generation should be from reservoir L to R , the effect of net electronic flow from the system into the reservoir L is to reduce the generated power and efficiency.

Once the ground state of G_1 is occupied, an electron existing in S_1 can either tunnel into S_2 giving rise to directional electronic flow or tunnel out to L without any net electron flow. Hence, the power output as well as efficiency of the proposed set-up hovers around 50% of the optimal design. To further understand the situation, in Fig. 5, I separate out the current flow into the system from the reservoir L depending on the occupation of ground state of the dot G_1 . In particular, Fig. 5(a) and (b) demonstrate the electron current flow into the system from reservoir L when the ground state of G_1 is unoccupied and occupied respectively. It should be noted that the electronic current demonstrated in Fig. 5, is opposite to the direction of conventional current flow. We find that when ε_g is unoccupied, the electron current flow into the system from L is positive or against the voltage bias, generating a net value of thermoelectric power. Interestingly, we also find that when the ground state of G_1 is occupied, the electronic current from L to S_1 is negative, that is, the net electron current flows into the reservoir from the system in the direction of voltage bias. It is evident that this component of electron current flow from the system into the reservoir L transmits heat packets, but impacts negatively on the generated power. Thus, this component of electron current impacts both the generated power and efficiency. The deterioration in the heat engine performance, due to the current component discussed above, can be alleviated by adding an extra filter between L and S_1 . However, doing so nullifies the novelty of the proposed set-up in terms of fabrication simplicity. In Fig. 5(c), I show the total electronic current flow from L to S_1 . The negative values of total electronic current corresponds to current flow in the direction of the applied bias, resulting no net thermoelectric power generation.

IV. CONCLUSION

To conclude, in this paper I have proposed a realistic design strategy for non-local heat engine based on Coulomb coupled systems. The performance of the proposed design was then theoretically analyzed and compared with the optimal set-up [5] using the QME approach. It was demonstrated that the proposed set-up outputs a maximum power of around 50% of the optimal set-up. However, the crucial advantage of the proposed design strategy is that along with a reasonable output power, it also circumvents the demand for a sharp step-like change in reservoir-to-system coupling, which is required for proper operation of the optimal set-up proposed in literature[5]. Although not shown here, the proposed system can also work as an efficient non-local heat engine when the reservoir G acts as a heat sink (cold) with respect to the reservoirs L and R (hot). In such a case, the direction of thermoelectric current flow is reversed. The various different possible design strategies

for non-local heat engines and their performance is left for future exploration. In addition, an investigation of the impact of electron-phonon interaction on the proposed design also constitutes an interesting research direction. Nevertheless, the set-up proposed in this paper can be

employed to fabricate high performance non-local heat engines using Coulomb coupled systems.

Acknowledgments: The author would like to thank Sponsored Research and Industrial Consultancy (IIT Kharagpur) for their financial support via grant no. IIT/SRIC/EC/MWT/2019-20/162.

[1] N. Walldorf, A.-P. Jauho, and K. Kaasbjerg, *Phys. Rev. B* **96**, 115415 (2017).

[2] A.-M. Daré, *Phys. Rev. B* **100**, 195427 (2019).

[3] Y. Zhang and J. Chen, *Physica E: Low-dimensional Systems and Nanostructures* **114**, 113635 (2019).

[4] A.-M. Daré and P. Lombardo, *Phys. Rev. B* **96**, 115414 (2017).

[5] R. Sánchez and M. Büttiker, *Phys. Rev. B* **83**, 085428 (2011).

[6] A. Singha, S. D. Mahanti, and B. Muralidharan, *AIP Advances* **5**, 107210 (2015).

[7] A. Singha and B. Muralidharan, *Scientific Reports* **7**, 7879 (2017).

[8] J. L. Mi, X. B. Zhao, T. J. Zhu, and J. P. Tu, *Journal of Physics D: Applied Physics* **41**, 205403 (2008).

[9] J.-F. Li, W.-S. Liu, L.-D. Zhao, and M. Zhou, *NPG Asia Mater* **2**, 152 (2010).

[10] S. Sumithra, N. J. Takas, W. M. Nolting, S. Sapkota, P. F. Poudeu, and K. L. Stokes, *Journal of Electronic Materials* **41**, 1401 (2012).

[11] J.-H. Bahk, Z. Bian, and A. Shakouri, *Phys. Rev. B* **87**, 075204 (2013).

[12] A. Agarwal and B. Muralidharan, *Applied Physics Letters* **105**, 013104 (2014).

[13] R. Kim and M. S. Lundstrom, *Journal of Applied Physics* **111**, 024508 (2012).

[14] R. Kim and M. S. Lundstrom, *Journal of Applied Physics* **110**, 034511 (2011).

[15] S. V. Faleev and F. m. c. Léonard, *Phys. Rev. B* **77**, 214304 (2008).

[16] N. Neophytou and H. Kosina, *Journal of Applied Physics* **114**, 044315 (2013).

[17] K. Uchida, H. Adachi, T. Kikkawa, A. Kirihara, M. Ishida, S. Yorozu, S. Maekawa, and E. Saitoh, *Proceedings of the IEEE* **104**, 1946 (2016).

[18] J. Sinova, S. O. Valenzuela, J. Wunderlich, C. H. Back, and T. Jungwirth, *Rev. Mod. Phys.* **87**, 1213 (2015).

[19] E. Saitoh, M. Ueda, H. Miyajima, and G. Tatara, *Applied Physics Letters* **88**, 182509 (2006).

[20] Y. Zhang, Y. Wang, C. Huang, G. Lin, and J. Chen, *Energy* **95**, 593 (2016).

[21] A. Hbel, J. Weis, W. Dietsche, and K. v. Klitzing, *Applied Physics Letters* **91**, 102101 (2007).

[22] I. H. Chan, R. M. Westervelt, K. D. Maranowski, and A. C. Gossard, *Applied Physics Letters* **80**, 1818 (2002).

[23] L. W. Molenkamp, K. Flensberg, and M. Kemerink, *Phys. Rev. Lett.* **75**, 4282 (1995).

[24] A. Singha, “Density matrix to quantum master equation (qme) model for arrays of coulomb coupled quantum dots in the sequential tunneling regime,” (2020), arXiv:2003.00522 [physics.app-ph].

[25] S. Datta, *Quantum Transport: Atom to Transistor* (Cambridge Press, 2005).

[26] M. Leijnse, M. R. Wegewijs, and K. Flensberg, *Phys. Rev. B* **82**, 045412 (2010).

[27] B. Sothmann, R. Sánchez, and A. N. Jordan, *Nanotechnology* **26**, 032001 (2014).

[28] N. Nakpathomkun, H. Q. Xu, and H. Linke, *Phys. Rev. B* **82**, 235428 (2010).

[29] J. Androulakis, K. Hsu, R. Pcionek, H. Kong, C. Uher, J. D’Angelo, A. Downey, T. Hogan, and M. Kanatzidis, *Advanced Materials* **18**, 1170 (2006).

[30] K. F. Hsu, S. Loo, F. Guo, W. Chen, J. S. Dyck, C. Uher, T. Hogan, E. K. Polychroniadis, and M. G. Kanatzidis, *Science* **303**, 818 (2004).

[31] Y. Pan, G. Hong, S. N. Raja, S. Zimmermann, M. K. Tiwari, and D. Poulikakos, *Applied Physics Letters* **106**, 093102 (2015).

[32] J. P. Feser, J. S. Sadhu, B. P. Azeredo, K. H. Hsu, J. Ma, J. Kim, M. Seong, N. X. Fang, X. Li, P. M. Ferreira, S. Sinha, and D. G. Cahill, *Journal of Applied Physics* **112**, 114306 (2012).

[33] B. L. Davis and M. I. Hussein, *Phys. Rev. Lett.* **112**, 055505 (2014).

[34] N. Mingo and D. A. Broido, *Phys. Rev. Lett.* **93**, 246106 (2004).

[35] N. Mingo, *Applied Physics Letters* **84**, 2652 (2004).

[36] F. Zhou, J. Szczech, M. T. Pettes, A. L. Moore, S. Jin, and L. Shi, *Nano Letters* **7**, 1649 (2007), pMID: 17508772.

[37] F. Zhou, A. L. Moore, M. T. Pettes, Y. Lee, J. H. Seol, Q. L. Ye, L. Rabenberg, and L. Shi, *Journal of Physics D: Applied Physics* **43**, 025406 (2010).

[38] A. I. Boukai, Y. Bunimovich, J. Tahir-Kheli, J.-K. Yu, W. A. Goddard, and J. R. Heath, *Nature* **451**, 168 (2008).

[39] A. I. Hochbaum, R. Chen, R. D. Delgado, W. Liang, E. C. Garnett, M. Najarian, A. Majumdar, and P. Yang, *Nature Publishing Group* **451**, 163 (2008).

[40] A. Balandin, A. Khitun, J. Liu, K. Wang, T. Borca-Tasciuc, and G. Chen, in *Eighteenth International Conference on Thermoelectrics* (1999) pp. 189–192.

[41] G. Chen, *Phys. Rev. B* **57**, 14958 (1998).

[42] R. S. Whitney, *Physical Review Letters* **112**, 130601 (2014).

[43] R. S. Whitney, *Phys. Rev. B* **91**, 115425 (2015).

[44] Y. Choi and A. N. Jordan, *Physica E: Low-dimensional Systems and Nanostructures* **74**, 465 (2015).